Mechanics of Advanced Composite Structures 5 (2018) 173 – 185

Semnan University

Mechanics of Advanced Composite Structures

journal homepage: http://MACS.journals.semnan.ac.ir

An Analytical Approach to Thermoelastic Bending of Simply Supported Advanced Ribbed Composite Plates

M. Shahravi[a], S. Fallahzade[b], M. Mokhtari[a,c*],

[a] *Department of Aerospace Engineering, Maleke Ashtar University of Technology, Tehran, Iran*
[b] *Department of Mechanical Engineering, Tehran, Iran*
[c] *Telecommunication department, Iranian space research center, Space research center, Tehran, Iran*

PAPER INFO

Paper history:
Received 2017-08-30
Received in revised form
2018-01-12
Accepted 2018-01-29

Keywords:
Ribbed composite plate
Thermoelastic bending
Laplace transform
Advanced composite

ABSTRACT

In the present paper, an analytical approach is used to study the thermal deflections of a simply supported composite plate with a beam-like stiffener. The results for a plate–beam system exposed to a sinusoidal thermal load is used to study the effects of the low Earth orbit (LEO) thermal conditions on the composite plates, which have been used in the structure of satellites and spacecraft. To solve the governing equations of the system, the Laplace transform method for the time domain is used with the Navier series expansions. As the employed method is completely analytical, the results are exact.

1. Introduction

Fibrous composites are widely used in many engineering structures that are subjected to severe thermal environments. The composites have many attractive properties, including temperature resistance and a low thermal coefficient of expansion. In fibrous composite laminates, the coefficients of thermal expansion in the direction of the fibers are usually much smaller than those in the transverse direction [1]. Therefore, several plate theories have been developed by various researchers to predict the correct bending behavior of composite laminates under mechanical/thermal loads. These plate theories have been reviewed in various studies [2-6]. Reddy [7] presented a thermal analysis of laminated composite plates using Kirchhoff's classical plate theory (CPT), Mindlin's first-order shear deformation theory (FSDT), and Reddy's higher-order shear deformation theory (HSDT) [8]. Tauchert [9] investigated the stationary two-dimensional temperature, stress, and displacement distributions for a simply supported slab consisting of bonded orthotropic layers. Khdeir and Reddy [10] developed refined plate theories to study the thermal stresses and deformations of cross-ply rectangular laminates using the state-stress approach. Savoia and Reddy [11] solved the transient heat conduction equation for a given temperature distribution across the thickness of laminates for a three-dimensional (3D) stress analysis of a square laminate subjected to a sudden uniform temperature change.

Rohwer et al. [12] obtained the thermal stresses in laminated composite plates using the higher-order theories. Carrera and Ciuffreda [13] obtained a closed-form solution for the thermal analysis of laminated composite plates using a unified formulation. A refined FSDT was presented and used for the thermal analysis of laminated structures without using a shear correction factor [14]. Zenkour [15] used the

* Corresponding author.
E-mail address: m_mokhtari@mut.ac.ir
DOI: 10.22075/MACS.2018.12357.1124

parabolic and trigonometric shear deformation theories for the thermomechanical analysis of cross-ply laminated composite plates. Zenkour et al. [16] extended the thermomechanical analysis of laminated composite plates resting on an elastic foundation. Zhen et al. [17] used the global–local higher-order theory to carry out a thermal analysis of a four-layered symmetric cross-ply laminated composite plate subjected to the actual temperature field. Gao and Zhao [18] developed the refined plate theory, which was based on the thermoelasticity theory, for the thermoelastic bending analysis of rectangular plates. Khdeir [19] obtained an exact solution for the thermoelastic bending analysis of cross-ply laminated arches with arbitrary boundary conditions. Kant and Shiyekar [20] developed an HSDT with a Taylor series-type expansion in the thickness direction of the displacements to analyze composite and sandwich plates under thermal loading. Noda et al. [21] provided various solution methods to solve 3D heat conduction problems; the temperature profiles for 1D, 2D, and 3D linear elastic bodies, such as beams, plates, and shells, were obtained by solving the respective Fourier heat conduction equation. However, a review of the literature showed that such solution techniques are rarely employed for the thermoelastic analysis of multilayered plates.

In recent years, the problems associated with thermomechanical deflections, bending, buckling, and vibrations of composite and functionally graded (FG) sandwich plates have been analyzed and solved by some authors using four-variable trigonometric shear deformation theories. Tounsi et al. [22] used a refined trigonometric shear deformation theory to analyze the thermoelastic bending of FG sandwich plates. Zidi et al. [23] used a four-variable refined plate theory for the bending analysis of functionally graded material (FGM) plates under hygro-thermo-mechanical loading. Beldjelili et al. [24] used a four-variable trigonometric plate theory to analyze the hygro-thermo-mechanical bending behavior of sigmoid (S)-FGM plates resting on various elastic foundations. Bouderba et al. [25, 26] developed a simple shear deformation theory to analyze the thermal stability of FG sandwich plates. Chikh et al. [27] performed a thermal buckling analysis of cross-ply laminated plates using a simplified HSDT.

Structures consisting of composite plates stiffened by a set of beams form a class of structural elements that have practical importance in various engineering applications, such as aircrafts and ships. Because aerospace and marine vehicles are subjected to thermal and dynamic loads, confident predictions of the natural frequencies and amplitudes of the vibrations of the structural components are essential for preventing excessive vibration levels, which may result in fatigue failure [28-30].

The addition of stiffeners to composite plates complicates the dynamic analysis and, thus, simplifying assumptions have to be made to facilitate a solution to the problem. Many analytical and numerical methods have been proposed to study the vibrations of rib-stiffened plates. The proposed approaches include the orthotropic [31] and grillage [32] models, the Lagrange multiplier formalism [33], the Rayleigh–Ritz method [34, 35], the finite difference method [36], the finite element method [37, 38], the differential quadrature method [39], and the meshless method [40]. Hygro-thermo-mechanical bendin analysis of S-FGM plates on variable elastic foundation studied by Beldjelili et al [41].

According to the literature, the thermomechanical bending analysis of ribbed composite plates has never been performed. Thus, the present study is the first attempt in using an analytical approach to solve the problem of thermal bending of a composite plate with a beam-like stiffener. To study the results, an applied case that occurs frequently in satellite structure design problems and has been never solved was considered. Assumptions of the CPT were considered to describe the motion of the composite plate [7], while the motion of the stiffener was assumed to follow the Euler–Bernoulli beam equation. To determine the relationship between the governing equations of the plate and stiffener, a compatibility equation was used [29]. In addition, the quasi-static equation of heat conduction was used to describe the temperature field of the plate. The plate and the beam were simply supported along the mechanical boundaries to allow a Fourier-type expansion of the Levy solution to be applied to trace the deflection of the composite plate in terms of the spatial coordinates. The thermal boundary condition on one side of the plate was considered to be in a sinusoidal form, which is common in LEO satellite applications. The temperature equation with the assumption of a small strain rate was uncoupled from the equation of motion of the plate by omitting the coupling term of displacement from the temperature equation. The quasi-static equation of heat conduction was solved separately using the Laplace transform method. Furthermore, the Laplace transform method was utilized to solve the system of governing equations of motion of the plate. Finally, the method of residues (residue theorem [41]) was applied to transform the algebraic results of the complex domain (s-domain) into the time domain. The solution method that is used in the present study is fully analytical and the results are exact within the framework of the CPT. Thus, this paper comprehensively investigates and graphically represents the effects of various parameters, such as the dimension of

the cross-section area of the stiffener and the orbital temperature parameters, on the time history bending of a composite plate and stiffener.

2. The Governing Equations of the Problem

2.1. Equations of Motion of a Composite Plate with a Stiffener

According to the CPT, the governing equations of motion of the composite plate may be written as follows in the absence of in-plane forces [7]:

$$\begin{aligned} &N_{xx,x}+N_{xy,y}=I_0\ddot{u}_0-I_1\ddot{w}_{0,x}\\ &N_{yx,x}+N_{yy,y}=I_0\ddot{v}_0-I_1\ddot{w}_{0,y}\\ &M_{xx,xx}+2M_{xy,xy}+M_{yy,yy}+q(x,y,t)\\ &\quad=I_0\ddot{w}_0+I_1\left(\ddot{u}_{0,x}+\ddot{v}_{0,y}\right)-I_2\left(\ddot{w}_{0,xx}+\ddot{w}_{0,yy}\right) \end{aligned} \tag{1}$$

where $(I_0,I_1,I_2)=\int_{-\frac{h}{2}}^{\frac{h}{2}}(1,\hat{z},\hat{z}^2)\rho_0 d\hat{z}$ and

$$\begin{aligned} \{N_{yy}\}&=\begin{bmatrix}A_{11}&A_{12}&A_{16}\\A_{12}&A_{22}&A_{26}\\A_{16}&A_{26}&A_{66}\end{bmatrix}\{v_{0,y}\}-\\ &\begin{bmatrix}B_{11}&B_{12}&B_{16}\\B_{12}&B_{22}&B_{26}\\B_{16}&B_{26}&B_{66}\end{bmatrix}\begin{Bmatrix}w_{0,xx}\\w_{0,yy}\\2w_{0,xy}\end{Bmatrix}-\begin{Bmatrix}N_{xx}^T\\N_{yy}^T\\N_{xy}^T\end{Bmatrix} \end{aligned} \tag{2}$$

$$\begin{aligned} \begin{Bmatrix}M_{xx}\\M_{yy}\\M_{xy}\end{Bmatrix}&=\begin{bmatrix}B_{11}&B_{12}&B_{16}\\B_{21}&B_{22}&B_{26}\\B_{61}&B_{62}&B_{66}\end{bmatrix}\begin{Bmatrix}u_{0,x}\\v_{0,y}\\u_{0,y}+v_{0,x}\end{Bmatrix}\\ &+\begin{bmatrix}D_{11}&D_{12}&D_{16}\\D_{21}&D_{22}&D_{26}\\D_{61}&D_{62}&D_{66}\end{bmatrix}\begin{Bmatrix}w_{0,xx}\\w_{0,yy}\\2w_{0,xy}\end{Bmatrix}-\begin{Bmatrix}M_{xx}^T\\M_{yy}^T\\M_{xy}^T\end{Bmatrix} \end{aligned} \tag{3}$$

where

$$\{N^T\}=\sum_{k=1}^{N}\int_{z_k}^{z_{k+1}}\left[\bar{Q}\right]^{(k)}\{\bar{\alpha}\}^{(k)}Tdz \tag{4}$$

$$\{M^T\}=\sum_{k=1}^{N}\int_{z_k}^{z_{k+1}}\left[\bar{Q}\right]^{(k)}\{\bar{\alpha}\}^{(k)}Tzdz \tag{5}$$

$$\left(A_{ij},B_{ij},D_{ij}\right)=\int_{-\frac{h}{2}}^{\frac{h}{2}}\bar{Q}_{ij}^{(k)}\left(1,\hat{z},\hat{z}^2\right)d\hat{z} \tag{6}$$

where $\hat{z}$ and z are measured from the mid-plane of the plate. The stiffener can be modeled as an Euler–Bernoulli beam parallel to the y-axis as shown in Fig. 1 assuming that the in-plane displacements u and v have no direct effect on the motion of the stiffener; the deflections of the plate are small; and the torsional interaction moment between the beam and the plate is negligible.

Therefore, the governing equation of the beam-like stiffener can be written as follows [34]:

$$EI\frac{\partial^4 w_1}{\partial x^4}+\rho A\frac{\partial^2 w_1}{\partial t^2}=f_1(x,t) \tag{7}$$

where w_1 is the deflection of the stiffener and $f_1(x,t)$ is the interaction force between the beam and the plate. Considering Equation (7) and neglecting the effect of the torsional interaction moment, the distributed transverse load $q(x,y,t)$ can be expressed as [22]:

$$q(x,y,t)=-f_1(x,t)\delta(y-y_1) \tag{8}$$

Substituting Equations (2), (3), and (8) into Equation (1) leads to the governing equations of the plate in terms of the displacement components:

$$\begin{aligned} &A_{11}\frac{\partial^2 u_0}{\partial x^2}+2A_{16}\frac{\partial^2 u_0}{\partial x\,\partial y}\\ &+A_{66}\frac{\partial^2 u_0}{\partial y^2}+A_{16}\frac{\partial^2 v_0}{\partial x^2}\\ &+\left(A_{12}+A_{66}\right)\frac{\partial^2 v_0}{\partial x\,\partial y}+A_{26}\frac{\partial^2 v_0}{\partial y^2}\\ &-\left[\begin{aligned}&B_{11}\frac{\partial^3 w_0}{\partial x^3}+3B_{16}\frac{\partial^3 w_0}{\partial x^2\partial y}+\\ &\left(B_{12}+2B_{66}\right)\frac{\partial^3 w_0}{\partial x\,\partial y^2}+B_{26}\frac{\partial^3 w_0}{\partial y^3}\end{aligned}\right]\\ &-\left(\frac{\partial N_{xx}^T}{\partial x}+\frac{\partial N_{xy}^T}{\partial y}\right)=I_0\ddot{u}_0-I_1\frac{\partial \ddot{w}_0}{\partial x} \end{aligned} \tag{9}$$

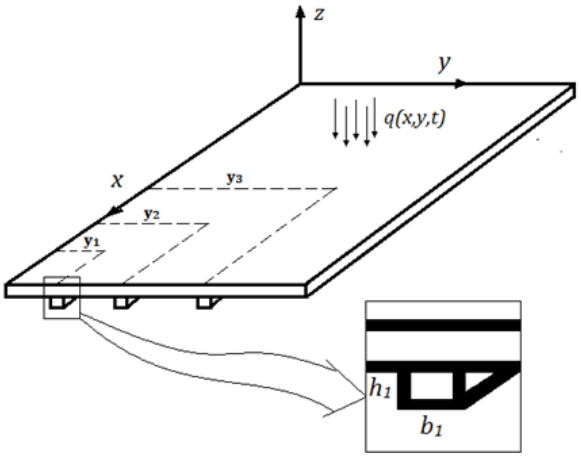

Figure 1 Schematic of a composite with parallel stiffeners

$$
\begin{aligned}
&A_{16}\frac{\partial^2 u_0}{\partial x^2}+\left(A_{12}+A_{66}\right)\frac{\partial^2 u_0}{\partial x\,\partial y}+A_{26}\frac{\partial^2 u_0}{\partial y^2}\\
&+A_{66}\frac{\partial^2 v_0}{\partial x^2}+2A_{26}\frac{\partial^2 v_0}{\partial x\,\partial y}+A_{22}\frac{\partial^2 v_0}{\partial y^2}\\
&-\left[\begin{array}{l}B_{16}\dfrac{\partial^3 w_0}{\partial x^3}+3B_{26}\dfrac{\partial^3 w_0}{\partial x\,\partial y^2}\\ +\left(B_{12}+2B_{66}\right)\dfrac{\partial^3 w_0}{\partial x^2\partial y}+B_{22}\dfrac{\partial^3 w_0}{\partial y^3}\end{array}\right]\\
&-\left(\frac{\partial N^T_{xy}}{\partial x}+\frac{\partial N^T_{yy}}{\partial y}\right)=I_0\ddot{v}_0-I_1\frac{\partial \ddot{w}_0}{\partial y}
\end{aligned}
\tag{10}
$$

$$
\begin{aligned}
&B_{11}\frac{\partial^3 u_0}{\partial x^3}+3B_{16}\frac{\partial^3 u_0}{\partial x^2\partial y}+\left(B_{12}+2B_{66}\right)\frac{\partial^3 u_0}{\partial x\,\partial y^2}\\
&+B_{26}\frac{\partial^3 u_0}{\partial y^3}+B_{16}\frac{\partial^3 v_0}{\partial x^3}+3B_{26}\frac{\partial^3 v_0}{\partial x\,\partial y^2}\\
&+\left(B_{12}+2B_{66}\right)\frac{\partial^3 v_0}{\partial x^2\partial y}+B_{22}\frac{\partial^3 v_0}{\partial y^3}\\
&-\left[\begin{array}{l}D_{11}\dfrac{\partial^4 w_0}{\partial x^4}+4D_{16}\dfrac{\partial^4 w_0}{\partial x^3\partial y}\\ +2\left(D_{12}+2D_{66}\right)\dfrac{\partial^4 w_0}{\partial x^2\partial y^2}\\ +4D_{26}\dfrac{\partial^4 u_0}{\partial x\,\partial y^3}+D_{22}\dfrac{\partial^4 w_0}{\partial y^4}\end{array}\right]\\
&+q-\left(\frac{\partial^2 M^T_{xx}}{\partial x^2}+\frac{\partial^2 M^T_{xy}}{\partial x\,\partial y}+\frac{\partial^2 M^T_{xy}}{\partial y^2}\right)\\
&=I_1\left(\frac{\partial \ddot{u}_0}{\partial x}+\frac{\partial \ddot{v}_0}{\partial y}\right)+I_0\ddot{w}_0-I_2\left(\frac{\partial^2 \ddot{w}_0}{\partial x^2}+\frac{\partial^2 \ddot{w}_0}{\partial y^2}\right)
\end{aligned}
\tag{11}
$$

Note that Equations (7) and (9)–(11) are the governing equations of motion of a composite plate with a beam-like stiffener. These equations must be solved in conjunction with the continuity condition at the interface between the plate and the beam, which can be expressed as follows [22]:

$$
w\left(x,y_1,t\right)=w_1\left(x,t\right) \tag{12}
$$

2.2 Heat Conduction and Temperature Distribution

In the present study, the quasi-static equation of heat conduction will be considered only for the plate. It has been assumed that the presence of the beam does not affect the heat conduction process. Thus, the quasi-static equation of heat conduction for a laminated composite plate can be written as follows [35]:

$$
\rho c\dot{T}=\left(k_{ij}T_{,j}\right)_i \tag{13}
$$

Assuming that the thermal properties of the plate are constant in any direction, Equation (13) can be expressed as:

$$
\frac{\partial^2 T}{\partial x^2}+\frac{\partial^2 T}{\partial y^2}+\frac{\partial^2 T}{\partial \bar{z}^2}=\frac{1}{\alpha_T}\frac{\partial T}{\partial t} \tag{14}
$$

where α is the coefficient of thermal diffusivity and $\bar{z}=z+h/2$. The boundary and initial conditions of Equation (14) are as follows:

$$
\begin{aligned}
&T\left(0,y,\bar{z},t\right)=T\left(a,y,\bar{z},t\right)\\
&\qquad=T\left(x,0,\bar{z},t\right)=T\left(x,b,\bar{z},t\right)=0\\
&T\left(x,y,0,t\right)=f\left(t\right),\\
&\qquad T\left(x,y,h,t\right)=0,T\left(x,y,\bar{z},0\right)=0
\end{aligned}
\tag{15}
$$

To solve Equation (14) with the prescribed boundary conditions of Equation (15), the following definition of the finite Fourier transform may be used in the $\bar{z}$ direction [41]:

$$
F_s\left[f\left(x\right);k\right]=\bar{f}_s\left(k\right)=\int_0^a f\left(x\right)\sin\left(\frac{k\pi x}{a}\right)dx \tag{16}
$$

The inverse transform may be obtained from

$$
F_s^{-1}\left[\bar{f}_s\left(k\right);x\right]=f\left(x\right)=\frac{2}{a}\sum_{k=1}^{\infty}\bar{f}_s\left(n\right)\sin\left(\frac{k\pi x}{a}\right) \tag{17}
$$

Employing the integration by parts rule, the following relation is derived based on the definition presented in Equation (16):

$$
\begin{aligned}
F_s\left[\frac{d^2 f}{dx^2};k\right]&=-\frac{k^2\pi^2}{a^2}\bar{f}_s\left(n\right)\\
&\quad+\frac{k\pi}{a}\left[\left(-1\right)^{k+1}f\left(a\right)+f\left(0\right)\right]
\end{aligned}
\tag{18}
$$

Applying the finite Fourier transform in the direction of $\bar{z}$ by making use of Equation (18) on Eqs. (14) and (15) leads to the following:

$$
\frac{\partial^2 T_k}{\partial x^2}+\frac{\partial^2 T_k}{\partial y^2}-\frac{k^2\pi^2}{h^2}T_k+\frac{k\pi}{h}f(t)=\frac{1}{\alpha_T}\frac{\partial T_k}{\partial t} \tag{19}
$$

$$
\begin{aligned}
&T_k\left(0,y,t\right)=T_k\left(a,y,t\right)\\
&\qquad=T_k\left(x,0,t\right)=T_k\left(x,b,t\right)=0
\end{aligned}
\tag{20}
$$

To satisfy the boundary condition, the double sinusoidal expansion of T_k will be used, which can be presented as follows:

$$T_k(x,y,t)=\sum_{m=1}^{\infty}\sum_{n=1}^{\infty}A_{mnk}(t)\sin\left(\frac{m\pi x}{a}\right)\sin\left(\frac{n\pi y}{b}\right) \quad (21)$$

Substituting $T_k(x,y,t)$ from Equation (21) into Equation (19) results in the following:

$$\frac{1}{\alpha}\frac{\partial A_{mnk}}{\partial t}+\left[\left(\frac{m\pi}{a}\right)^2+\left(\frac{n\pi}{b}\right)^2+\left(\frac{k\pi}{h}\right)^2\right]A_{mnk} =\frac{k}{mn\pi}\frac{ab}{h}f(t)\left[1-\cos(n\pi)\right]\left[1-\cos(n\pi)\right] \quad (22)$$

Applying the Laplace transform to Equation (22) gives the Laplace transform version of A_{mnk} as follows:

$$\bar{A}_{mnk}=\frac{k}{mn\pi}\frac{ab}{h}\frac{\bar{F}(s)[1-\cos(n\pi)][1-\cos(n\pi)]}{\left(\frac{m\pi}{a}\right)^2+\left(\frac{n\pi}{b}\right)^2+\left(\frac{k\pi}{h}\right)^2+\frac{s}{\alpha_T}} \quad (23)$$

where $\bar{A}_{mnk}(s)=L\left(A_{mnk}(t)\right)$ and $\bar{F}(s)=L\left(f(t)\right)$. Making use of the inverse Fourier transform of Equation (17) with Equation (21) results in the following:

$$T(x,y,\bar{z},t)=\sum_{k=1}^{\infty}T_k(x,y,t)\sin\left(\frac{k\pi\bar{z}}{h}\right) =\sum_{m=1}^{\infty}\sum_{n=1}^{\infty}\sum_{k=1}^{\infty}A_{mnk}(t) \times\sin\left(\frac{k\pi\bar{z}}{h}\right)\sin\left(\frac{m\pi x}{a}\right)\sin\left(\frac{n\pi y}{b}\right) \quad (24)$$

Therefore,

$$T(x,y,\bar{z},t)=\sum_{m=1}^{\infty}\sum_{n=1}^{\infty}T_{mn}(\bar{z},t) \times\sin\left(\frac{m\pi x}{a}\right)\sin\left(\frac{n\pi y}{b}\right) \quad (25)$$

where

$$T_{mn}(\bar{z},t)=\sum_{k=1}^{\infty}A_{mnk}(t)\sin\left(\frac{k\pi\bar{z}}{h}\right) \quad (26)$$

In the following sections, Equations (4) and (5) in the form of $T(x,y,\bar{z},t)$, which has been presented in Equation (25), will be used to calculate the thermal force vector $\{N^T\}$ and the thermal moment vector $\{M^T\}$.

3. Analytical Solution of the Governing Equations

The simply supported boundary conditions for the classical linear plate theory are as follows:

$$\begin{aligned} &u_0(x,0,t)=0,\ u_0(x,b,t)=0,\\ &\qquad v_0(0,y,t)=0,\ v_0(a,y,t)=0\\ &w_0(x,0,t)=0,\ w_0(x,b,t)=0,\\ &\qquad w_0(0,y,t)=0,\ w_0(a,y,t)=0\\ &w_{0,x}(x,0,t)=0,\ w_{0,x}(x,b,t)=0,\\ &\qquad w_{0,y}(0,y,t)=0,\ w_{0,y}(a,y,t)=0 \end{aligned} \quad (27)$$

$$\begin{aligned} &N_{xx}(0,y,t)=0,\ N_{xx}(a,y,t)=0,\\ &\qquad N_{yy}(x,0,t)=0,\ N_{yy}(x,b,t)=0\\ &M_{xx}(0,y,t)=0,\ M_{xx}(a,y,t)=0,\\ &\qquad M_{yy}(x,0,t)=0,\ M_{yy}(x,b,t)=0 \end{aligned} \quad (28)$$

The boundary conditions in Equation (27) may be satisfied using the following Navier-type solutions:

$$\begin{aligned} u_0(x,y,t)&=\sum_{n=1}^{\infty}\sum_{m=1}^{\infty}U_{mn}(t)\cos(\alpha x)\sin(\beta y)\\ v_0(x,y,t)&=\sum_{n=1}^{\infty}\sum_{m=1}^{\infty}V_{mn}(t)\sin(\alpha x)\cos(\beta y)\\ w_0(x,y,t)&=\sum_{n=1}^{\infty}\sum_{m=1}^{\infty}W_{mn}(t)\sin(\alpha x)\sin(\beta y) \end{aligned} \quad (29)$$

where $\alpha=m\pi/a$ and $\beta=n\pi/b$. $q(x,y,t)$ may also be expressed in the following double Fourier series:

$$q(x,y,t)=\sum_{m=1}^{\infty}\sum_{n=1}^{\infty}Q_{mn}(t)\sin\left(\frac{m\pi x}{a}\right)\sin\left(\frac{n\pi y}{b}\right) \quad (30)$$

where

$$Q_{mn}(t)=\frac{4}{ab}\int_0^a\int_0^b q(x,y,t) \times\sin\left(\frac{m\pi x}{a}\right)\sin\left(\frac{n\pi y}{b}\right)dxdy \quad (31)$$

Substituting $q(x,y,t)$ from Equation (8) into Equation (31) leads to the following:

$$Q_{mn}(t)=-\frac{4}{ab}F_m^1\sin\left(\frac{n\pi y_1}{b}\right) \quad (32)$$

where

$$F_m^1=\int_0^a f_1(x,t)\sin\left(\frac{m\pi x}{a}\right)dx \quad (33)$$

After the displacements of Equation (29) are first inserted into Equations (2) and (3), and then inserted into Equation (28), the result reveals that the Navier

solution of Equation (29) exists only if $A_{16} = A_{26} = B_{16} = B_{26} = D_{16} = D_{26} = A_{45} = 0,\ I_1 = 0$.

It follows that the Navier solution for simply supported boundary conditions applies to plates with the following characteristics: a single generally orthotropic layer; symmetrically laminated plates with multiple orthotropic layers; and antisymmetric cross-ply laminated plates, which include the former cases as special cases. Substituting the Navier solution of Equation (29) into the governing Equations (9–11) leads to the following equation in terms of the unknown coefficients of the Navier solution U_{mn}, V_{mn}, W_{mn}:

$$\sum_{n=1}^{\infty}\sum_{m=1}^{\infty}\begin{pmatrix} -\left(A_{11}\alpha^2 + A_{66}\beta^2\right)U_{mn} \\ -\left(A_{12}+A_{66}\right)\alpha\beta V_{mn} \\ +\left(B_{11}\alpha^3 + B_{12}\alpha\beta^2\right)W_{mn} \\ -I_0\ddot{U}_{mn} + I_1\alpha\ddot{W}_{mn} \end{pmatrix} \times\cos(\alpha x)\sin(\beta y) = \left(\frac{\partial N_{xx}^T}{\partial x} + \frac{\partial N_{xy}^T}{\partial y}\right) = f_1^T \tag{34}$$

$$\sum_{n=1}^{\infty}\sum_{m=1}^{\infty}\begin{pmatrix} -\left(A_{12}+A_{66}\right)\alpha\beta U_{mn} \\ -\left(A_{11}\alpha^2 + A_{66}\beta^2\right)V_{mn} \\ +\left(B_{12}\alpha^2\beta + B_{22}\beta^3\right)W_{mn} \\ -I_0\ddot{V}_{mn} + I_1\beta\ddot{W}_{mn} \end{pmatrix} \times\sin(\alpha x)\cos(\beta y) = \left(\frac{\partial N_{xy}^T}{\partial x} + \frac{\partial N_{yy}^T}{\partial y}\right) = f_2^T \tag{35}$$

$$\sum_{n=1}^{\infty}\sum_{m=1}^{\infty}\begin{bmatrix} -\left(B_{11}\alpha^3 + B_{12}\alpha\beta^2\right)U_{mn} \\ -\left(B_{12}\alpha^2\beta + B_{22}\beta^3\right)V_{mn} \\ -\left(D_{11}\alpha^4 + 2D_{12}\alpha^2\beta^2 + D_{22}\beta^4\right)W_{mn} \\ -I_1\alpha\ddot{U}_{mn} - I_1\beta\ddot{V}_{mn} \\ +\left(I_0 + I_2\left(\alpha^2+\beta^2\right)\right)\ddot{W}_{mn} \end{bmatrix} \times\sin(\alpha x)\sin(\beta y) = \left(\frac{\partial^2 M_{xx}^T}{\partial x^2} + \frac{\partial^2 M_{xy}^T}{\partial x\,\partial y} + \frac{\partial^2 M_{xy}^T}{\partial y^2}\right) - q(x,y,t) = f_3^T - q(x,y,t) \tag{36}$$

where $\tilde{B}_{12} = B_{12} + 2B_{66}$ and $\tilde{D}_{12} = D_{12} + 2D_{66}$.

Expanding the thermal force vectors N_{ij}^T and the thermal moment vectors M_{ij}^T in terms of the double Fourier sries leads to:

$$\begin{Bmatrix} N_{xx}^T \\ N_{yy}^T \\ N_{xy}^T \end{Bmatrix} = \sum_{m=1}^{\infty}\sum_{n=1}^{\infty}\begin{Bmatrix} N_{mn}^1 \\ N_{mn}^2 \\ N_{mn}^6 \end{Bmatrix}\sin(\alpha x)\sin(\beta y) \tag{38}$$

$$\begin{Bmatrix} M_{xx}^T \\ M_{yy}^T \\ M_{xy}^T \end{Bmatrix} = \sum_{m=1}^{\infty}\sum_{n=1}^{\infty}\begin{Bmatrix} M_{mn}^1 \\ M_{mn}^2 \\ M_{mn}^6 \end{Bmatrix}\sin(\alpha x)\sin(\beta y) \tag{39}$$

where

$$\begin{Bmatrix} N_{mn}^1 \\ N_{mn}^2 \\ N_{mn}^6 \end{Bmatrix} = \sum_{k=1}^{N}\int_{z_k}^{z_{k+1}}\left[\overline{Q}\right]^{(k)}\left\{\overline{\alpha}\right\}T_{mn}(z,t)\,dz \tag{40}$$

$$\begin{Bmatrix} M_{mn}^1 \\ M_{mn}^2 \\ M_{mn}^6 \end{Bmatrix} = \sum_{k=1}^{N}\int_{z_k}^{z_{k+1}}\left[\overline{Q}\right]^{(k)}\left\{\overline{\alpha}\right\}T_{mn}(z,t)\,z\,dz \tag{41}$$

Note that $T_{mn}(z,t)$ has been defined by Equation (26). The temperature-related terms in the governing Equations (9)–(11) can then be written as follows:

$$f_1^T = \frac{\partial N_{xx}^T}{\partial x} + \frac{\partial N_{xy}^T}{\partial y} = \sum_{n=1}^{\infty}\sum_{m=1}^{\infty}[\alpha N_{mn}^1\cos(\alpha x)\sin(\beta y) + \beta N_{mn}^6\sin(\alpha x)\cos(\beta y)] \tag{42}$$

$$f_2^T = \frac{\partial N_{xy}^T}{\partial x} + \frac{\partial N_{yy}^T}{\partial y} = \sum_{n=1}^{\infty}\sum_{m=1}^{\infty}[\alpha N_{mn}^6\cos(\alpha x)\sin(\beta y) + \beta N_{mn}^1\sin(\alpha x)\cos(\beta y)] \tag{43}$$

$$f_3^T = \frac{\partial^2 M_{xx}^T}{\partial x^2} + \frac{\partial^2 M_{xy}^T}{\partial x\,\partial y} + \frac{\partial^2 M_{xy}^T}{\partial y^2} = \sum_{n=1}^{\infty}\sum_{m=1}^{\infty}[-\left(\alpha^2 M_{mn}^1 + \beta^2 M_{mn}^2\right)\sin(\alpha x)\sin(\beta y) + 2\alpha\beta M_{mn}^6\cos(\alpha x)\cos(\beta y)] \tag{44}$$

The particular form of the solution of the problem, which is based on the double Fourier series, re-

quires that M_{mn}^6 and N_{mn}^6 be defined to achieve an analytical solution. Thus, the configuration of the composite plate must be as follows:

$$\sum_{k=1}^{N}\int_{z_k}^{z_{k+1}}\left[\overline{Q}\right]^{(k)}\left\{\overline{\alpha}\right\}T_{mn}(z,t)dz=\begin{Bmatrix}N_{mn}^{1}\\N_{mn}^{2}\\0\end{Bmatrix} \tag{45}$$

$$\sum_{k=1}^{N}\int_{z_k}^{z_{k+1}}\left[\overline{Q}\right]^{(k)}\left\{\overline{\alpha}\right\}T_{mn}(z,t)zdz=\begin{Bmatrix}M_{mn}^{1}\\M_{mn}^{2}\\0\end{Bmatrix} \tag{46}$$

The conditions in Equations (45) and (46) are automatically satisfied for the following conditions: single-layer plates with a generally orthotropic layer; symmetrically laminated plates with multiple orthotropic layers; and antisymmetric cross-ply laminated plates. In order to include N_{mn}^6 and M_{mn}^6, the temperature distribution should be expanded in a double cosine series. Then N_{mn}^1, N_{mn}^2, M_{mn}^1, and M_{mn}^2 must be equal to zero [7]. Substituting f_1^T, f_2^T, and f_3^T from Equations (42)–(44) into Equations (34)–(36) results in the following governing equations of motion of the plate:

$$\begin{bmatrix}\hat{c}_{11}&\hat{c}_{12}&\hat{c}_{13}\\\hat{c}_{12}&\hat{c}_{22}&\hat{c}_{23}\\\hat{c}_{13}&\hat{c}_{23}&\hat{c}_{33}\end{bmatrix}\begin{Bmatrix}U_{mn}\\V_{mn}\\W_{mn}\end{Bmatrix}+\begin{bmatrix}\hat{m}_{11}&0&0\\0&\hat{m}_{22}&0\\0&0&\hat{m}_{33}\end{bmatrix}\begin{Bmatrix}\ddot{U}_{mn}\\\ddot{V}_{mn}\\\ddot{W}_{mn}\end{Bmatrix}=\begin{Bmatrix}0\\0\\-\frac{4}{ab}F_m^1\sin(\beta y_1)\end{Bmatrix}+\begin{Bmatrix}-\alpha N_{mn}^{1}\\-\beta N_{mn}^{2}\\\alpha^2M_{mn}^{1}+\beta^2M_{mn}^{2}\end{Bmatrix} \tag{47}$$

in which

$$\begin{aligned}\hat{c}_{11}&=\left(A_{11}\alpha^2+A_{66}\beta^2\right)\\\hat{c}_{12}&=\left(A_{12}+A_{66}\right)\alpha\beta\\\hat{c}_{13}&=-\left(B_{11}\alpha^3+B_{12}\alpha\beta^2\right)\\\hat{c}_{22}&=\left(A_{66}\alpha^2+A_{22}\beta^2\right)\\\hat{c}_{23}&=-\left(B_{12}\alpha^2\beta+B_{22}\beta^3\right)\\\hat{c}_{33}&=\left(D_{11}\alpha^4+2D_{12}\alpha^2\beta^2+D_{22}\beta^4\right)\\\hat{m}_{11}&=\hat{m}_{22}=I_0\\\hat{m}_{33}&=\left(I_0+I_2\left(\alpha^2+\beta^2\right)\right)\end{aligned} \tag{48}$$

Equations (7) and (48) are the governing equations of the system shown in Fig. (1), and must be solved simultaneously. The lateral deflection of the beam may be presented as follows:

$$w_1(x,t)=\sum_{m=1}^{\infty}W_m^1(t)\sin\left(\frac{m\pi x}{a}\right) \tag{49}$$

Substituting $w_1(x,t)$ from Equation (49) into Equation (7) results in the following equation for the motion of the stiffener:

$$EI\left(\frac{m\pi}{a}\right)^4W_m^1(t)+\rho A\ddot{W}_m^1(t)=\frac{2}{a}F_m^1 \tag{50}$$

where

$$F_m^1=\int_0^a f_1(x,t)\sin\left(\frac{m\pi x}{a}\right)dx \tag{51}$$

Equations (47) and (50) are the coupled equtations governing the motion of the system of a composite plate with a beam-like stiffener, which must be solved in conjunction with the continuity condition that has been expressed in Equation (7). In order to solve Equations (47) and (50), the Laplace transform may be employed. Assuming that all of the initial conditions are zero, after the Laplace transform is applied, the form of the governing equations will be as follows:

$$\left(\begin{bmatrix}\hat{c}_{11}&\hat{c}_{12}&\hat{c}_{13}\\\hat{c}_{12}&\hat{c}_{22}&\hat{c}_{23}\\\hat{c}_{13}&\hat{c}_{23}&\hat{c}_{33}\end{bmatrix}+s^2\begin{bmatrix}\hat{m}_{11}&0&0\\0&\hat{m}_{22}&0\\0&0&\hat{m}_{33}\end{bmatrix}\right)\begin{Bmatrix}\overline{U}_{mn}\\\overline{V}_{mn}\\\overline{W}_{mn}\end{Bmatrix}=\begin{Bmatrix}0\\0\\-\frac{4}{ab}\overline{F}_m^1\sin(\beta y_1)\end{Bmatrix}+\begin{Bmatrix}-\alpha\overline{N}_{mn}^{1}\\-\beta\overline{N}_{mn}^{2}\\\alpha^2\overline{M}_{mn}^{1}+\beta^2\overline{M}_{mn}^{2}\end{Bmatrix} \tag{52}$$

$$\phi_m\overline{W}_m^1=\frac{2}{a}\overline{F}_m^1 \tag{53}$$

where

$$\phi_m=EI\left(\frac{m\pi}{a}\right)^4+\rho As^2 \tag{54}$$

Substituting $\overline{F}_m^1$ from Equation (53) into Equation (52) leads to

$$\left(\begin{bmatrix}\hat{c}_{11} & \hat{c}_{12} & \hat{c}_{13}\\ \hat{c}_{12} & \hat{c}_{22} & \hat{c}_{23}\\ \hat{c}_{13} & \hat{c}_{23} & \hat{c}_{33}\end{bmatrix}+s^2\begin{bmatrix}\hat{m}_{11} & 0 & 0\\ 0 & \hat{m}_{22} & 0\\ 0 & 0 & \hat{m}_{33}\end{bmatrix}\right)\times\begin{Bmatrix}\overline{U}_{mn}\\ \overline{V}_{mn}\\ \overline{W}_{mn}\end{Bmatrix}=\begin{Bmatrix}0\\ 0\\ -\frac{2}{b}\phi_m\overline{W}^1_m\sin(\beta y_1)\end{Bmatrix}+\begin{Bmatrix}-\alpha\overline{N}^1_{mn}\\ -\beta\overline{N}^2_{mn}\\ \alpha^2\overline{M}^1_{mn}+\beta^2\overline{M}^2_{mn}\end{Bmatrix} \quad (55)$$

The Laplace transform version of Equation (12) is

$$\overline{W}^1_m(s)=\overline{W}_m(y_1,s) \quad (56)$$

Based on the Fourier series expansions, the following relations are valid:

$$\overline{W}(x,y,s)=\sum_{m=1}^{\infty}\overline{W}_m(y,s)\sin\left(\frac{m\pi x}{a}\right) \quad (57)$$

$$\overline{W}_m(y,s)=\sum_{n=1}^{\infty}\overline{W}_{mn}(s)\sin\left(\frac{n\pi y}{b}\right) \quad (58)$$

From Equations (55) and (56) we have

$$\begin{Bmatrix}\overline{U}_{mn}\\ \overline{V}_{mn}\\ \overline{W}_{mn}\end{Bmatrix}=\begin{bmatrix}\varphi_{11} & \varphi_{12} & \varphi_{13}\\ \varphi_{12} & \varphi_{22} & \varphi_{23}\\ \varphi_{13} & \varphi_{23} & \varphi_{33}\end{bmatrix}\begin{Bmatrix}0\\ 0\\ -\frac{2}{b}\phi_m\overline{W}_m(y_1,s)\sin(\beta y_1)\end{Bmatrix}+\begin{bmatrix}\varphi_{11} & \varphi_{12} & \varphi_{13}\\ \varphi_{12} & \varphi_{22} & \varphi_{23}\\ \varphi_{13} & \varphi_{23} & \varphi_{33}\end{bmatrix}\begin{Bmatrix}-\alpha\overline{N}^1_{mn}\\ -\beta\overline{N}^2_{mn}\\ \alpha^2\overline{M}^1_{mn}+\beta^2\overline{M}^2_{mn}\end{Bmatrix} \quad (59)$$

where

$$\begin{bmatrix}\varphi_{11} & \varphi_{12} & \varphi_{13}\\ \varphi_{12} & \varphi_{22} & \varphi_{23}\\ \varphi_{13} & \varphi_{23} & \varphi_{33}\end{bmatrix}=\left(\begin{bmatrix}\hat{c}_{11} & \hat{c}_{12} & \hat{c}_{13}\\ \hat{c}_{12} & \hat{c}_{22} & \hat{c}_{23}\\ \hat{c}_{13} & \hat{c}_{23} & \hat{c}_{33}\end{bmatrix}+s^2\begin{bmatrix}\hat{m}_{11} & 0 & 0\\ 0 & \hat{m}_{22} & 0\\ 0 & 0 & \hat{m}_{33}\end{bmatrix}\right)^{-1} \quad (60)$$

The third row of Equation (59) can be written as

$$\overline{W}_{mn}=-\psi^1_{mn}\overline{W}_m(y_1,s)+\psi^2_{mn} \quad (61)$$

where

$$\psi^1_{mn}=\frac{2}{b}\varphi_{33}\phi_m\sin(\beta y_1) \quad (62)$$

$$\psi^2_{mn}=-\alpha\overline{N}^1_{mn}\varphi_{13}-\beta\overline{N}^2_{mn}\varphi_{23}+\left(\alpha^2\overline{M}^1_{mn}+\beta^2\overline{M}^2_{mn}\right)\varphi_{33} \quad (63)$$

Substituting Equation (61) into Equation (58) results in the following:

$$\overline{W}_m(y,s)=\sum_{n=1}^{\infty}\left(-\psi^1_{mn}\overline{W}_m(y_1,s)+\psi^2_{mn}\right)\sin\left(\frac{n\pi y}{b}\right) \quad (64)$$

Replacing y with y_1 on both sides of Equation (64) leads to the following expression for $\overline{W}_m(y_1,s)$:

$$\overline{W}_m(y_1,s)=\frac{\Psi^2_m(y_1,s)}{1+\Psi^1_m(y_1,s)} \quad (65)$$

where

$$\Psi^1_m(y_1,s)=\sum_{n=1}^{\infty}\psi^1_{mn}\sin\left(\frac{n\pi y_1}{b}\right) \quad (66)$$

$$\Psi^2_m(y_1,s)=\sum_{n=1}^{\infty}\psi^2_{mn}\sin\left(\frac{n\pi y_1}{b}\right) \quad (67)$$

Substituting $\overline{W}_m(y,s)$ from Equation (65) into Equation (59), and then substituting the results into the Laplace transform version of Equation (29) leads to the Laplace transform version of the displacement components $\overline{U}_0(x,y,s)$, $\overline{V}_0(x,y,s)$, and $\overline{W}_0(x,y,s)$. By making use of the inverse Laplace transform, the Navier solution (29) for $u_0(x,y,t)$, $v_0(x,y,t)$, and $w_0(x,y,t)$ may be obtained in the time domain. The inverse Laplace transform of $\overline{U}_0(x,y,s)$, $\overline{V}_0(x,y,s)$, and $\overline{W}_0(x,y,s)$ is determined using Maple software and the residue theorem. In order to successfully accomplish the process of applying the inverse Laplace transform to any rational function using the residue theorem [37], the roots of the denominator must be found. In the case of Equation (30), the most challenging part of the denominator is $1+\Psi^1_m(y_1,s)$. However, the series of $\Psi^1_m(y_1,s)$ converges rapidly by the growth in the number of terms. Thus, the roots of $1+\Psi^1_m(y_1,s)$ can be found for any desired degree of accuracy and can be used in the implementation of the residue theorem.

4. Results and Discussions

In this the section, different aspects of the current problem and the effects of various parameters, including the periodic thermal load and the stiffener, on the results will be discussed in detail using some numerical examples. In this regard, consider a symmetrically laminated [0/90/90/0] composite plate with the following specifications:

$$E_1 = 144.8 \text{ GPa}, \quad E_2 = 9.65 \text{ GPa},$$
$$G_{12} = 4.136 \text{ GPa}, \quad \nu_{12} = 0.25,$$
$$\rho = 1389.297 \text{ Kg/m}^3$$

The thickness of each layer is 1 mm and the dimensions of this plate are 0.4 m × 0.4 m; the mass of the plate would be 0.889 kg. Thus, according to Equation 6, the non-zero coefficients of this plate are:

$$A_{11} = 3.101920206\times10^8, \quad A_{12} = 9.690362568\times10^6,$$
$$A_{22} = 3.101920206\times10^8, \quad A_{66} = 1.654400000\times10^7$$
$$D_{11} = 685.0199, \quad D_{12} = 19.3807,$$
$$D_{22} = 213.2381, \quad D_{66} = 33.0880,$$
$$I_0 = 5.557, \quad I_2 = 0.000007$$

The plate has a stiffener with a cross-section area of $b_1 \times h_1$ (Fig. 1), which is attached to the plate in $y_1 = b/2$. It has the following mechanical and thermal properties:

$$E = 144.8 \text{ GPa}, \quad \nu = 0.3, \quad \rho = 1389.297 \ \frac{\text{Kg}}{\text{m}^3};$$
$$\alpha = 1.165\times10^{-4} \text{ (for carbon/epoxy composites);}$$
$$\begin{Bmatrix}\alpha_{11}\\ \alpha_{22}\\ \alpha_{12}\end{Bmatrix} = \begin{Bmatrix}2.1\times10^{-6}\\ 2.1\times10^{-6}\\ 0\end{Bmatrix}\frac{1}{K^o}$$

where α is the thermal diffusivity coefficient of the composite plate with the assumption of homogeneity and α_{ij} is the thermal expansion coefficient of the composite plate.

Furthermore, suppose that a sinusoidal temperature $f(t) = B\sin(\omega t)$ has been applied to the upper surface of the plate; in this case, the sinusoidal temperature is applied to the stiffened composite plates of the outer surface of the structure of a LEO satellite. In the equation, B is the amplitude of the temperature and ω is the frequency of the temperature function. In the case of an LEO satellite, it takes about 90 minutes (an orbital period) to complete a revolution in its orbit around Earth. The effects of B and ω on the temperature of the midpoint of the stiffened plate are shown in Fig. 2, which result from Equations (24) and (25). Tracing the temperature variation through the thickness suggests that using a linear approximation of temperature for many applied purposes would result in an acceptable precision. However, in this study, the exact solution of the thermal conduction equation has been used to achieve higher levels of accuracy.

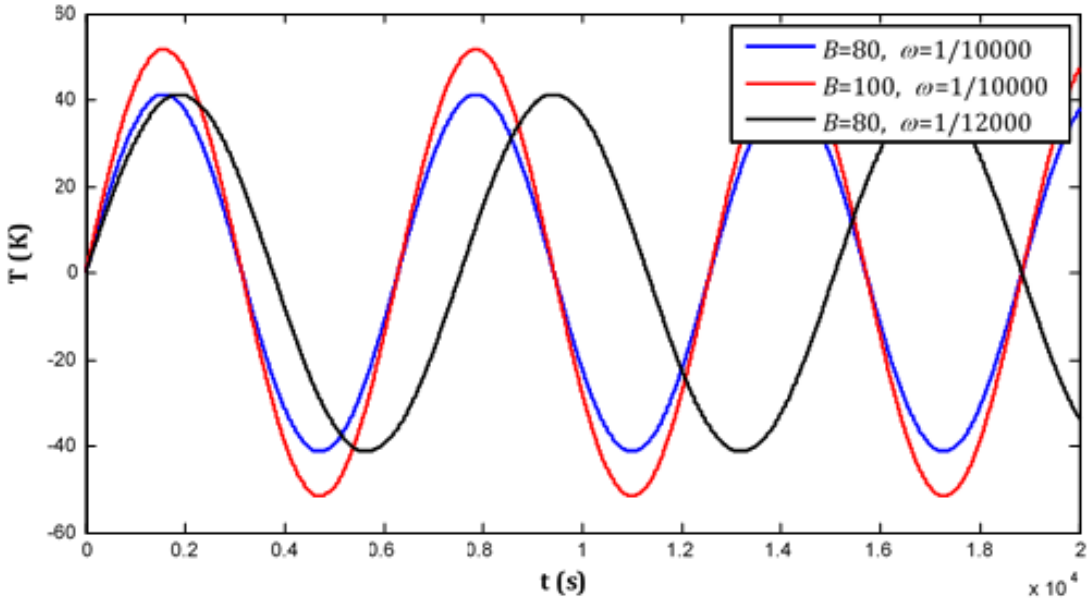

Figure 2. Effects of the orbital temperature parameters of B and ω on the temperature at the midpoint of the composite plate ($\boldsymbol{x} = \frac{\boldsymbol{a}}{\boldsymbol{2}}, \boldsymbol{y} = \frac{\boldsymbol{b}}{\boldsymbol{2}}$) with a stiffener ($b_1 = 0.01$ m, $h_1 = 0.02$ m)

Fig. 3 shows the effect of the height of the stiffener, which is an important parameter, on the time history deflection of the midpoint of the plate. As can be deduced from Fig. 3, using a stiffener with a relatively small height will not diminish the amplitude of the deflection of the plate to a considerable extent. Therefore, to decrease the amplitude considerably, the height of the stiffener (beam) must be comparable with the plate's thickness (i.e., more than 2 times larger). Fig. 4 shows the effect of the stiffener's height on the maximum deflection of the plate. This illustration also shows that a stiffener with a relatively small height does not significantly affect the maximum amplitude of the plate and that the sensitivity of the amplitude to the height of the stiffener increases as the height of the stiffener increases. However, the case for the width ($\boldsymbol{b_1}$) of the cross-section area of the plate is quite different. For example, Fig. 4 shows the effect of the stiffener's width on the maximum deflection of the plate. As can be seen in the figure, the decrease in the maximum deflection of the plate with respect to $\boldsymbol{b_1}$ has almost a linear pattern. This is because of the moment of inertia of the cross-section area of the beam with respect to its neutral axis ($\boldsymbol{I = 1/12 b_1 h_1^3}$), which is a linear function of $\boldsymbol{b_1}$ and a cubic function of $\boldsymbol{h_1}$. This means that for a constant cross-section area, the beam should have a high $\boldsymbol{h_1}$ and a low $\boldsymbol{b_1}$ to reduce the maximum deflection of the beam. Of course we have to keep in mind that a beam with very low $\boldsymbol{b_1}$ may cause high degrees of stress concentration, which must be avoided for design purposes (see Fig. 5).

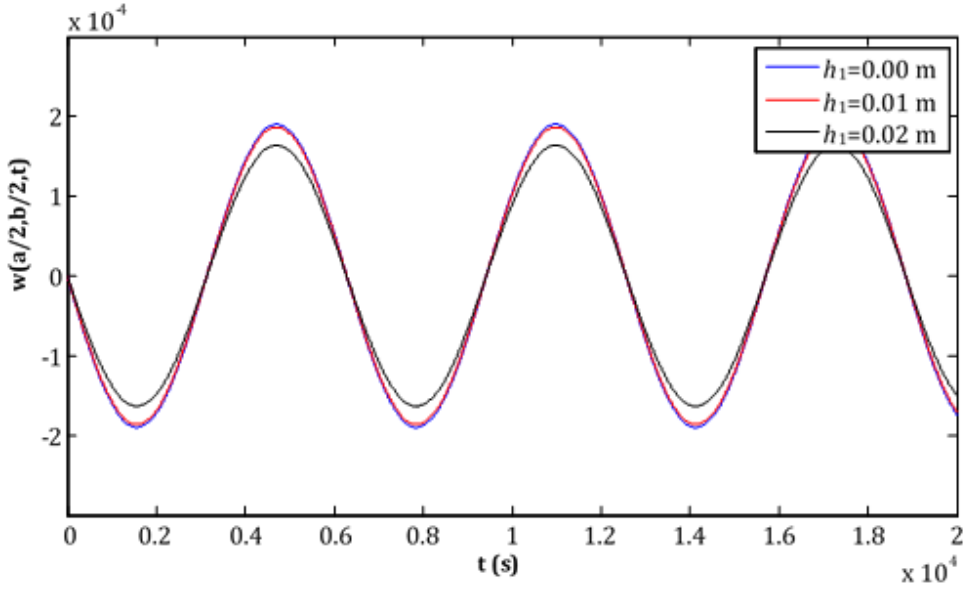

Figure 3. Effect of the height of the stiffener (h_1) on the time-history deflection of the midpoint of the plate for $b_1 = 0.02$ m

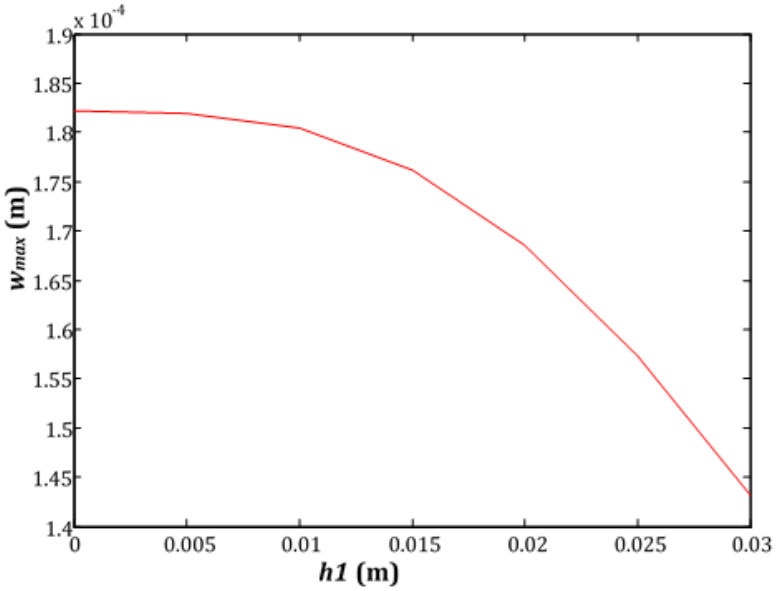

Figure 4. Effect of h_1 of the stiffener on the maximum amplitude of the deflection of the midpoint of the plate for b_1=0.01 m

In Fig. 6, the effect of B and ω on the deflection of the midpoint of the composite plate ($x = a/2, y = b/2$) with $b_1 = 0.01, h_1 = 0.02$ is shown. Note that all the figures have been produced under the assumption that the inner space of the satellite is at a constant temperature. However, this is an optimistic assumption for the electronic devices that are inside the satellite and a pessimistic assumption for the plate deflection because it results in greater deflections. In real-life situations, such an assumption cannot be fulfilled because the inner temperature of the satellite will probably change with the environment as the satellite moves in front of the sun in its orbit. Thus, the actual deflections will be less than the deflections presented in this paper.

5. Conclusion

In the present paper, an analysis of the thermal deflections of a simply supported ribbed composite plate with application in LEO satellite structures is accomplished for the first time. By employing the CPT description to explain the behavior of the composite laminated plate, exact results are extracted for the time histories and an analysis of the effects of various parameters is presented and illustrated graphically.

In addition to the novelties presented in the modeling and solution stages, some of the practical conclusions that have been drawn may be summarized as follows:

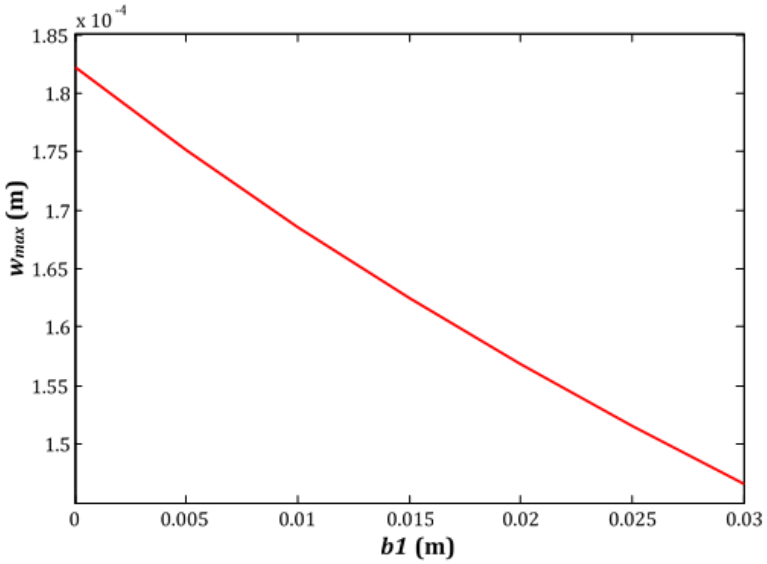

Figure 5. Effect of b_1 of the stiffener on the maximum amplitude of deflection of the midpoint of the plate for $h_1 = 0.02$ m

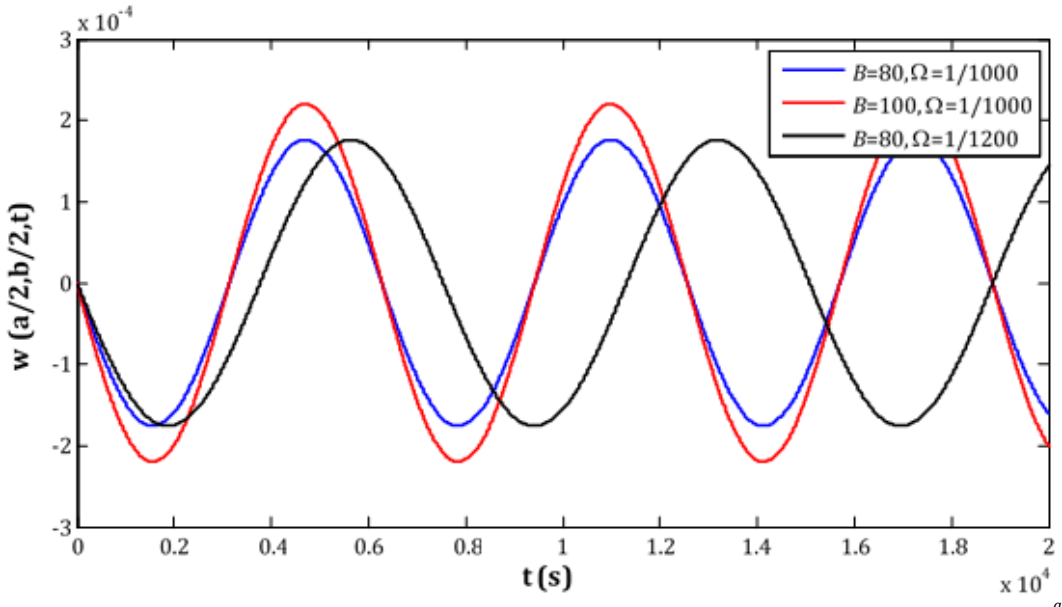

Figure 6. Effects of the orbital temperature parameters of B and ω on the deflection of the midpoint of the composite plate ($x = \frac{a}{2}, y = \frac{b}{2}$) with a stiffener ($b_1 = 0.01$ m, $h_1 = 0.02$ m).

- The presented method is analytical and, thus, it is computationally fast and the results are exact. These properties make the method useful in recursive optimization algorithms, which can be used to provide a basis for the design of composite satellite structures with stiffeners for use in the harsh LEO environment.
- The effects of the width and height of a stiffener with a rectangular cross-section area on the time history of thermoelastic bending of the composite plate have been comprehensively investigated and it has been deduced that a stiffener with a larger height is more effective than a smaller stiffener.
- Finally, the effects of the orbital temperature parameters of B and ω on the deflection of the midpoint of the composite plate have been illustrated. The results showed that there is a linear relation between the maximum temperature of the environment and the maximum deflection of the plate.

References

[1] Sayyad AS, Ghugal YM, Mhaske BA. A Four-Variable Plate Theory for Thermoelastic Bending Analysis of Laminated Composite Plates, *Journal of Thermal Stresses* 2015; 38: 904–925.

[2] Tauchert TR, Thermally Induced Flexure, Buckling and Vibration of Plates. *Appl. Mech. Rev.* 1991; 44(8):347–360.

[3] Argyris J, Tenek L. Recent Advances in Computational Thermostructural Analysis of Composite Plates and Shells with Strong Nonlinearities. *Appl. Mech. Rev.* 1997; 50(5): 285–306.

[4] Kant T, Swaminathan K. Estimation of Transverse/Interlaminar Stresses in Laminated Composites—A Selective Review and Survey of Current Developments. *Compos. Struct.* 2000; 49: 65–75.

[5] Reddy JN, Arciniega RA. Shear Deformation Plate and Shell Theories: From Stavsky to Present. *Mech. Adv. Mater. Struct.* 2004; 11(6): 535–582.

[6] Wanji C, Zhen W. A Selective Review on Recent Development of Displacement-Based Laminated Plate Theories. *Recent Pat. Mech. Eng.* 2008; 1:29–44.

[7] Reddy JN, **Mechanics of Laminated Composite Plates**, CRC Press, Boca Raton, 1997.

[8] Reddy JN, A Simple Higher Order Theory for Laminated Composite Plates, *ASME J. Appl. Mech.* 1984; 51: 745–752.

[9] Tauchert TR. Thermoelastic Analysis of Laminated Orthotropic Slabs. *J. Therm. Stresses* 1980; 3: 117–132.

[10] Khdeir AA, Reddy JN, Thermal Stresses and Deflections of Cross Ply Laminated Plates Using Refined Plate Theories. *J. Therm. Stresses* 1991; 14: 419–439.

[11] Savoia M, Reddy JN. Three-Dimensional Thermal Analysis of Laminated Composite Plates, *Int. J. Solids Struct.* 1995; 32: 593–608.

[12] Rohwer K, Rolfes R, Sparr H. Higher-Order Theories for Thermal Stresses in Layered Plates, *Int. J. Solids Struct*. 2001; 38: 3673–3687.

[13] Carrera E, A Ciuffred. Closed-Form Solutions to Assess Multilayered-Plate Theories for Various Thermal Stress Problems. *J. Therm. Stresses* 2004; 27: 1001–1031.

[14] Fares ME, Zenkour AM. Mixed Variational Formula for the Thermal Bending of Laminated Plates. *J. Therm. Stresses.* 1999; 22: 347–365.

[15] Zenkour AM. Analytical Solution for Bending of Cross-Ply Laminated Plates under Thermo-Mechanical Loading. *Compos. Struct.* 2004; 65: 367–379.

[16] Zenkour AM, Allam MNM, Radwan AF. Bending of Cross-Ply Laminated Plates Resting on Elastic Foundations under Thermo-Mechanical Loading. *Int. J. Mech. Mater. Des.* 2013; 9: 239–251.

[17] Zhen W, Cheng YK, Lo SH, Chen W. Thermal Stress Analysis For Laminated Plates Using Actual Temperature Field. *Int. J. Mech. Sci.* 2007; 49: 1276–1288.

[18] Gao Y, Zhao B. The Refined Theory of Thermoelastic Rectangular Plates. *J. Therm. Stresses* 2007; 30: 505–520.

[19] Khdeir AA. An Exact Solution for the Thermoelastic Deformations of Cross-Ply Laminated Arches with Arbitrary Boundary Conditions. *J. Therm. Stresses.* 2011; 34: 1227–1240.

[20] Kant T, Shiyekar SM. An Assessment of a Higher Order Theory for Composite Laminates Subjected to Thermal Gradient. *Compos. Struct.* 2013; 96: 698–707.

[21] Noda N, Hetnarski RB, Tanigawa Y, **Thermal Stresses**, 2nd Edition, Taylor & Francis: New York; 2003.

[22] Tounsi A, Houari MSA, Benyoucef S. A refined trigonometric shear deformation theory for thermoelastic bending of functionally graded sandwich plates. *Aerospace Sci. Tech.* 2013; 24: 209-220.

[23] Zidi M, Tounsi A, Houari MSA, Bég OA. Bending analysis of FGM plates under hygro-thermo-mechanical loading using a four variable refined plate theory. *Aerospace Sci. Tech.* 2014; 34: 24-34.

[24] Beldjelili Y, Tounsi A, Mahmoud SR. Hygro-thermo-mechanical bending of S-FGM plates resting on variable elastic foundations using a four-variable trigonometric plate theory. *Smart Struct. Syst., Int. J.* 2016; 18(4): 755-786.

[25] Bouderba B, Houari MS, Tounsi A, Mahmoud SR. Thermal stability of functionally graded sandwich plates using a simple shear deformation theory. *Structural Engineering, Mechanics* 2016; 58(3): 397-422.

[26] Bousahla AA, Benyoucef S, Tounsi A, Mahmoud SR. On thermal stability of plates with functionally graded coefficient of thermal expansion. *Struct. Eng. Mech.* 2016; 60(2): 313-335.

[27] Chikh A, Tounsi A, Hebali H, Mahmoud SR. Thermal buckling analysis of cross-ply laminated plates using a simplified HSDT, *Smart Structures Systems* 2017; 19(3): 289-297.

[28] Dozio L, Ricciardi M. Free vibration analysis of ribbed plates by a combined analytical–numerical method. *Journal of Sound and Vibration* 2009; 319: 681–697.

[29] Ney SF, Kulkarni GG. On the transverse free vibration of beam-slab type highway bridges. *Journal of Sound and Vibration* 1972; 21: 249–261.

[30] Attia A, Tounsi A, Bedia EA, Mahmoud SR. Free vibration analysis of functionally graded plates with temperature-dependent properties using various four variable refined plate theories. *Steel and composite structures* 2015; 18(1):187-212.

[31] Balendra T, Shanmugam NE. Free vibration of plate structures by grillage method. *Journal of Sound and Vibration* 1985; 99: 333–350.

[32] Dowell EH. Free vibrations of an arbitrary structure in terms of component modes. *Journal of Applied Mechanics* 1972; 39: 727–732.

[33] Liew KM, Xiang Y, Kitipornchai S, Meek JL. Formulation of Mindlin–Engesser model for stiffened plate vibration. *Computer Methods in Applied Mechanics and Engineering* 1995; 120(3–4): 339–353.

[34] Berry A, Locqueteau C. Vibration and sound radiation of fluid-loaded stiffened plates with consideration of in-plane deformation. *Journal of the Acoustical Society of America* 1996; 100 (1): 312–319.

[35] Asku G, Ali R. Free vibration analysis of stiffened plates using finite difference method. *Journal of Sound and Vibration* 1976; 48: 15–25.

[36] Bhimaraddi A, Carr AJ, Moss PJ. Finite element analysis of laminated shells of revolution with laminated stiffeners. *Computers and Structures* 1989; 33: 295–305.

[37] Harik IE, Guo M. Finite element analysis of eccentrically stiffened plates in free vibration. *Computers and Structures* 1993; 49: 1007–1015.

[38] Zeng H, Bert CW. A differential quadrature analysis of vibration for rectangular stiffened plates. *Journal of Sound and Vibration* 2001; 241: 247–252.

[39] Rao SS. **Vibration of Continuous Systems**. Wiley; Hoboken: 2007.

[40] Hetnarski RB, Eslami MR, Gladwell GML, **Thermal stresses: advanced theory and applications**. Springer: 2009.

[41] Spiegel MR. **Advanced Mathematics for Engineers and Scientists**. New York: McGraw-Hill; 1971.

[42] Sneddon IN, **The use of integral transforms**, McGraw-Hill; 1972.